Catalysis Science & Technology

Accepted Manuscript

ROYAL SOCIETY OF CHEMISTRY

www.rsc.org/catalysis

CO Oxidative Coupling to DMO

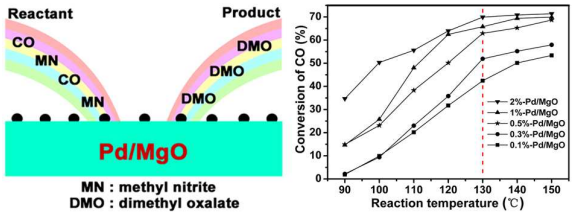

We firstly found that the basic MgO can serve as an excellent support used in the Pd catalyst for CO oxidative coupling to DMO, and further developed a low Pd loading (*ca.*0.5 wt%) Pd/MgO catalyst with high activity, selectivity and stability.

Cite this: DOI: 10.1039/c0xx00000x

www.rsc.org/xxxxxx

ARTICLE TYPE

MgO: an excellent catalyst support for CO oxidative coupling to dimethyl oxalate†

Si-Yan Peng,[a,b] Zhong-Ning Xu,*[a] Qing-Song Chen,[a] Zhi-Qiao Wang,[a] Yu-Min Chen,[a] Dong-Mei Lv,[a] Gang Lu,[a] Guo-Cong Guo*[a]

Received (in XXX, XXX) Xth XXXXXXXXX 20XX, Accepted Xth XXXXXXXXX 20XX
DOI: 10.1039/b000000x

Pd/MgO catalysts are found, for the first time, to be extraordinarily active and stable for CO oxidative coupling to dimethyl oxalate. A series of Pd/MgO catalysts with Pd loadings of 0.1, 0.3, 0.5, 1 and 2 wt% were prepared by a wet impregnation method and systematically characterized by XRD, TEM, ICP, UV-DRS, H_2-TPR and CO_2-TPD. It has been demonstrated that the amount of Pd loading has a pronounced effect on the catalytic activity for CO oxidative coupling to dimethyl oxalate. CO conversion increases with the increase of the Pd loading due to the high dispersion and the similar size of Pd nanoparticles, as well as the increase of surface active sites.

1. Introduction

Dimethyl oxalate (DMO) is an important chemical raw material and intermediate for the syntheses of oxalic acid, oxamide, dyes, pharmaceuticals, etc.[1] More importantly, hydrogenation of DMO can also be used to synthesize ethylene glycol (EG),[2-5] which is a considerable chemical feedstock with a global demand of about 25 million tons each year. Commercial EG is mainly produced from ethylene oxide hydrolysis.[6] Considering the soaring price of crude oil and the depletion of petroleum resources, a new EG synthesis technology called coal to ethylene glycol (CTEG) developed by our institute is attracting growing interest because of its green and atomic economy.[7, 8] CTEG contains three main processes: 1) elimination small amount of hydrogen gas in CO separated from coal-derived synthesis gas; 2) CO oxidative coupling to DMO: $2CH_3ONO+2CO \rightarrow (COOCH_3)_2+2NO$; 3) hydrogenation of DMO to EG. Among which, CO oxidative coupling to DMO is the crucial step to realize the conversion of inorganic C1 to organic C2 in CTEG.[9]

Pd/α-Al_2O_3 has been widely considered to be active catalyst for CO oxidative coupling to DMO.[10-14] Hoverever, there are still several problems to be solved despite considerable efforts have been dedicated to the study of CO oxidative coupling process. To date, the Pd loading of industrial catalyst for CO oxidative coupling to DMO is relatively high at 2 wt% (the state of the art), resulting in the cost of production greatly increased. Moreover, the catalytic mechanism of CO oxidative coupling to DMO remains controversial. Pd based catalysts supported on other supports with high activity for CO oxidative coupling to DMO are rather limited. Pd catalysts with different supports for CO oxidative coupling to DMO have been summarized by Uchiumi et al, and the results have demonstrated that Pd catalysts supported on NaY zeolite, silica, activated alumina, activated carbon show much lower activities compared to Pd/α-Al_2O_3.[15] Zhao et al.[1] reported a high efficiency Pd based catalyst supported on carbon nanofiber for the synthesis of DMO, but the Pd loading of the catalyst is still much higher (1 wt%). It is well established that support effect has a significant influence on many heterogeneous catalytic reactions, such as CO oxidation,[16, 17] methane combustion,[18] hydrogenation of nitrobenzene,[19] ethylene oxidation,[20] and acrylonitrile decomposition.[21] Acid-base and redox properties of the support and metal-support interaction can greatly affect the catalytic performances of supported catalysts. Therefore, designing efficient Pd based nanocatalysts by making use of support effect is necessary and important from points of view of both fundamental study and industry application.

It is desirable and practical to develop high performance Pd based catalysts supported on other supports for CO oxidative coupling to DMO. In this work, we firstly discovered a distinguished MgO support and further developed a low Pd loading (*ca.*0.5 wt%) Pd/MgO catalyst with high activity, selectivity and stability for CO oxidative coupling to DMO.

2. Experimental

2.1. Catalyst preparation

A series of Pd/MgO catalysts with 0.1, 0.3, 0.5, 1 and 2% (by weight) Pd loadings were prepared by a wet impregnation method and controlling the amount of palladium acetate precursor. MgO support was impregnated with an acetone solution of palladium acetate under vigorous magnetic stirring, and then the mixed

[a] *State Key Laboratory of Structural Chemistry, Fujian Institute of Research on the Structure of Matter, Chinese Academy of Sciences, Fuzhou, Fujian 350002, P. R. China. E-mail: gcguo@fjirsm.ac.cn; Fax: +86-591-83714946; Tel: +86-591-83512502*

[b] *Key Laboratory of Coal to Ethylene Glycol and Its Related Technology, Chinese Academy of Sciences, Fuzhou, Fujian 350002, P. R. China*

solution was heated at 50 °C until the acetone was evaporated away completely. The sample was calcined at 400 °C for 4 h to form PdO/MgO. Prior to the activity evaluation, the calcined sample was reduced in hydrogen atmosphere to obtain Pd/MgO. The calcined samples were denoted as 0.1%-PdO/MgO, 0.3%-PdO/MgO, 0.5%-PdO/MgO, 1%-PdO/MgO and 2%-PdO/MgO, respectively, and the reduced catalysts were thus denoted as 0.1%-Pd/MgO, 0.3%-Pd/MgO, 0.5%-Pd/MgO, 1%-Pd/MgO and 2%-Pd/MgO, respectively.

Other supported Pd catalysts such as Pd/α-Al_2O_3, Pd/TiO_2, Pd/γ- Al_2O_3 and Pd/AC (activated charcoal) were prepared by the same method for comparison. The theoretic Pd loadings of these catalysts were all 0.5 wt%, and the actual Pd loadings were measured by Inductively Coupled Plasma (ICP).

2.2. Catalyst characterization

Powder X-ray diffraction (XRD) patterns were measured on a glass wafer by a Rigaku MiniFlex II diffractometer with a Cu-Kα X ray source (λ = 1.5406 Å) at scan speed of 5°/min (2θ). The X-ray tube was operated at 40 kV and 30 mA. Samples for transmission electron microscopy (TEM) observations were prepared by drying a drop of diluted ethanol dispersion of Pd/MgO catalysts on copper grids. Images were obtained on a TEM (Tecnai G^2 F20) operated at 200 kV. ICP elemental analysis measurements were carried out on an Ultima2 plasma emission spectrometer from Jobin Yvon. UV-visible diffuse reflectance spectra (UV–DRS) were measured on a PE Lambda 950 spectrophotometer equipped with a diffuse reflectance accessory, and were recorded in the range of 400–850 nm using $BaSO_4$ as reference sample. Temperature programmed reduction (TPR) and temperature programmed desorption (TPD) of CO_2 experiments were carried out using Altamira AMI-300 instrument equipped with a thermal conductivity detector (TCD). Prior to conducting the H_2-TPR experiment, 100 mg sample placed in a quartz U-tube was first heated to 400 °C for 1 h in a flow of argon (30 mL/min). After cooled to room temperature, the sample was exposed to 10% H_2/Ar mixture (30 mL/min), and then heated to 500 °C at a rate of 10 °C/min. The basic properties of catalysts were examined by CO_2-TPD technique. In a typical experiment, 100 mg sample was treated in helium at 400 °C for 2 h to remove the adsorbed impurities. After cooled to 25 °C in helium flow, the sample was exposed to 40% CO_2/He mixture (50 mL/min) for 1 h, followed by purging with helium for 30 min, and then heated to 800 °C by ramping at 10 °C/min under flowing helium.

2.3. Activity evaluation

The activities of the catalysts for CO oxidative coupling to DMO were carried out in a fixed-bed quartz tubular reactor. The catalysts (200 mg) were placed in the center of quartz tubular reactor. The reactant gases (28% CO, 20% CH_3ONO, 4% Ar and N_2 balance) were passed through the reactor at a gas hourly space velocity (GHSV) of 3000 h^{-1}. The catalytic activity tests were performed under atmospheric pressure. The composition of the reactant gases and reaction products was monitored by an on-line Shimadzu GC-2014 gas chromatography equipped with a thermal conductivity detector and a flame ionization detector.

The conversion of CO, the selectivity to DMO and the space-time yields (STY) of DMO were calculated using the following formulas:

Conversion of CO (%) = $(1-([Ar]_{in}/[Ar]_{out})/([CO]_{in}/[CO]_{out})) \times 100\%$

Selectivity to DMO (%) = $(S_{DMO} \times R\text{-}F_{DMO})/(S_{DMO} \times R\text{-}F_{DMO} + S_{DMC} \times R\text{-}F_{DMC}) \times 100\%$

STY of DMO ($gL^{-1}h^{-1}$) = Conversion of CO × Selectivity to DMO × GHSV of CO × 118.09 $g{\cdot}mol^{-1}/(2 \times 22.4\ L{\cdot}mol^{-1})$

Where $[Ar]_{in}$ and $[Ar]_{out}$ are the concentrations of Ar at the inlet and outlet, $[CO]_{in}$ and $[CO]_{out}$ are the concentrations of CO at the inlet and outlet, respectively. S_{DMO} and S_{DMC} are the peak areas of dimethyl oxalate and dimethyl carbonate, R-F_{DMO} and R-F_{DMC} are the relative correction factors of dimethyl oxalate and dimethyl carbonate, respectively.

3. Results and discussion

3.1 Catalytic activity

The evaluation of catalytic performance for CO oxidative coupling to DMO was carried out in a home-made catalytic evaluation device. Table 1 summarizes the catalytic performances for CO oxidative coupling to DMO over Pd/MgO, Pd/α-Al_2O_3, Pd/TiO_2, Pd/γ-Al_2O_3 and Pd/AC catalysts, which were prepared by the same method and evaluated with the same reaction conditions. It is interesting to find that Pd/MgO exhibits remarkable catalytic performance for CO oxidative coupling to DMO even exceeding that of Pd/α-Al_2O_3, whereas other supported catalysts show much lower activities for this reaction. The CO oxidative coupling activity is in the order of Pd/MgO > Pd/α-Al_2O_3 > Pd/TiO_2 > Pd/γ-Al_2O_3 > Pd/AC, which demonstrates that the catalytic activity for CO oxidative coupling to DMO is strongly dependent on the nature of the support materials.

Table 1 CO oxidative coupling to DMO on different catalysts.[a]

Catalysts	Actual Pd loading (%)	Conversion [b] (%)	Selectivity [c] (%)	STY [d] ($gL^{-1}h^{-1}$)
Pd/MgO	0.42	63	97	1353
Pd/α-Al_2O_3	0.46	56	94	1166
Pd/TiO_2	0.43	26	90	518
Pd/γ- Al_2O_3	0.41	20	88	390
Pd/AC	0.42	15	89	296

[a] Reaction conditions: 200 mg of catalyst, theoretic Pd loading of 0.5 wt%, 3000 h^{-1} of gas hourly space velocity (GHSV), reactants CO/CH_3ONO volume ratio 1.4, 0.1 MPa, 130 °C. [b] Conversion of CO. [c] Selectivity to DMO. [d] STY represents the space-time yield, grams of DMO per liter of catalyst per hour ($gL^{-1}h^{-1}$).

Fig. 1 shows CO conversion over Pd/MgO catalysts with different Pd loadings as a function of reaction temperature. The temperature dependence of CO conversion indicates that the activities of Pd/MgO catalysts for CO oxidative coupling to DMO increase gradually as the temperature is raised from 90 to 150 °C. Besides, the amount of Pd loading has also a significant influence on the catalytic activity for CO oxidative coupling to DMO. By and large, CO conversion increases with the increase of the Pd loading, but not in proportion to it. However, the high Pd loading will result in the cost of catalysts greatly increased due to the expensive price and extreme shortage of Pd noble metal. The 0.5%-Pd/MgO catalyst exhibits high activity and selectivity with 63% CO conversion and 97% selectivity to DMO

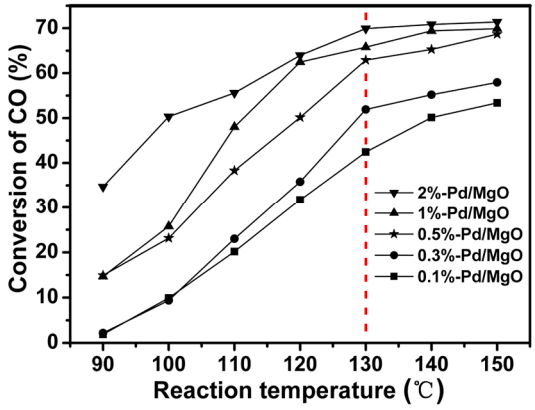

Fig. 1 Conversion of CO over Pd/MgO catalysts with different Pd loadings for CO oxidative coupling to DMO at different reaction temperatures.

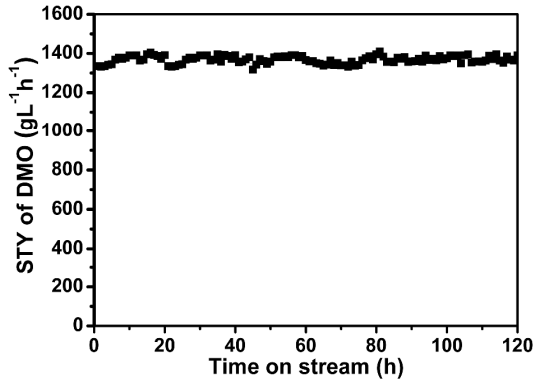

Fig. 2 Space-time yield of DMO over 0.5%-Pd/MgO catalyst (200 mg) at 130 °C for 120 h.

under the same reaction conditions of industrial catalyst. Moreover, CO conversion can reach up to 68.7% at 150 °C, close to the theoretical maximum value of 71.4%. Therefore, a Pd loading around 0.5 wt% is identified as an optimum content from both catalytic performance and economical points of view. The stability investigation of 0.5%-Pd/MgO catalyst has been carried out with a duration lifetime test for 120 h at 130 °C. As shown in Fig. 2, the excellent catalytic performance can be stable over 120 h, which lays a good foundation for further enlarging a long-term stability test. Furthermore, Pd/MgO was prepared via a wet impregnation method, which is flexible in controlling the Pd loading and suitable for its large-scale production.

3.2 Catalyst characterization

Fig. 3 presents the TEM images and the size-distribution histograms of Pd/MgO catalysts. Obviously, the Pd nanoparticles of all catalysts are highly dispersed on the surface of MgO support, suggesting that the Pd nanoparticles are not aggregated with the increase of the Pd loading. The number of Pd nanoparticles increases significantly with the increase of the Pd loading, but the average size of the Pd nanoparticles remains nearly unchanged. The average sizes of the Pd nanoparticles over all catalysts are located between 4.1–4.5 nm. It should be mentioned that the size statistics of 0.1%-Pd/MgO catalyst can not be obtained since few Pd nanoparticles can be observed (Fig. 3a). However, the size of the existing Pd nanoparticles over 0.1%-Pd/MgO catalyst is similar to those of other catalysts. In addition, the size distributions of Pd nanoparticles over all catalysts are much narrow and uniform, and show no marked differences. Therefore, the active sites will increase as the Pd loading increases from 0.1 to 2 wt%, which contributes mainly to

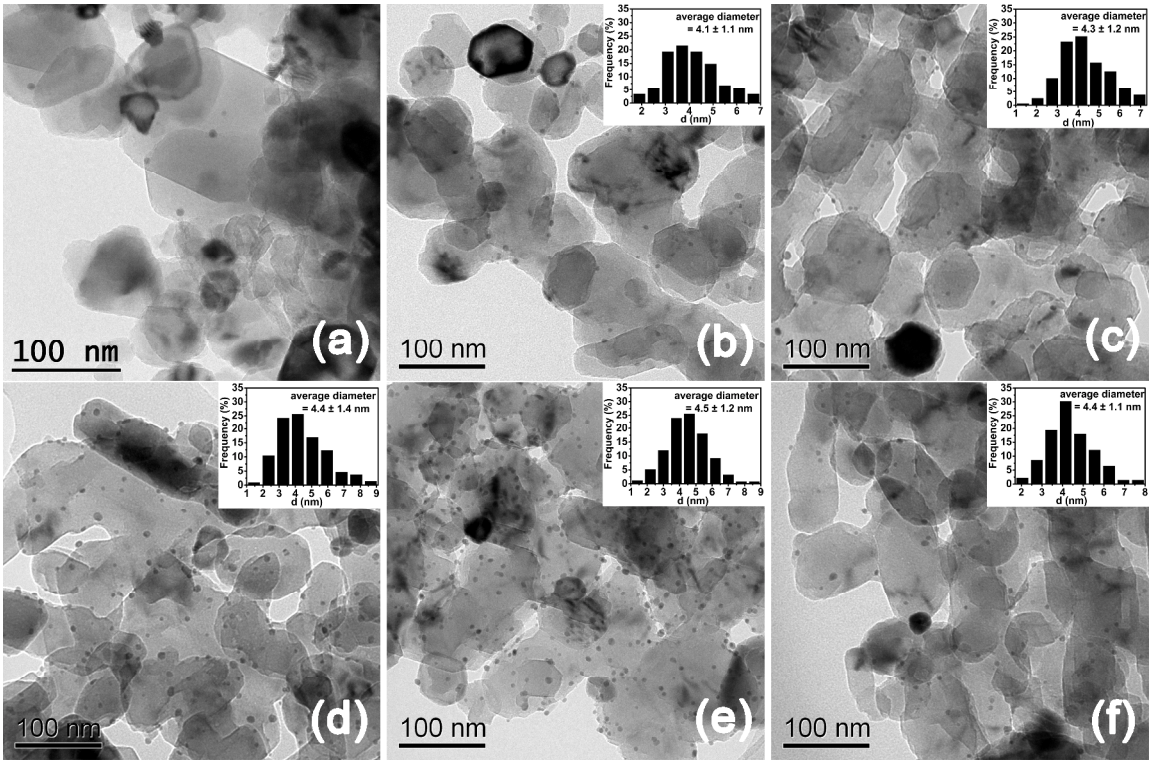

Fig. 3 TEM images of 0.1%-Pd/MgO (a), 0.3%-Pd/MgO (b), 0.5%-Pd/MgO (c), 1%-Pd/MgO (d), 2%-Pd/MgO (e), and 0.5%-Pd/MgO after 120 h lifetime evaluation (f). The insets are corresponding to the size distributions of Pd nanoparticles supported on MgO.

the increasing catalytic activity for CO oxidative coupling to DMO (Fig. 1). It should be noted that the morphology and the size distribution of Pd nanoparticles of 0.5%-Pd/MgO after the durability test for 120 h (Fig. 3f) are very similar to those of the fresh catalyst (Fig. 3c). This implies that neither aggregation nor sintering of the Pd nanoparticles for 0.5%-Pd/MgO occured during the lifetime evaluation process, which illustrates the high stability of 0.5%-Pd/MgO catalyst.

Fig. 4 shows the XRD patterns of Pd/MgO catalysts with different Pd loadings. The sharp diffraction peaks are observed for all the five catalysts at 2θ = 37.1, 43.1, 62.4, 74.8, and 78.6°, which are assigned to the crystalline phase of the MgO support.[22] No Pd diffraction peaks are observed for 0.1%-Pd/MgO, 0.3%-Pd/MgO, 0.5%-Pd/MgO and 1%-Pd/MgO catalysts, indicating that the Pd nanoparticles are highly dispersed on the surface of MgO or the amounts of Pd loading are too small to be detected. When the Pd loading is raised to 2 wt%, there is a new weak diffraction peak at 40° observed for 2%-Pd/MgO catalyst, corresponding to the face-centered cubic (fcc) Pd (111) characteristic diffraction.

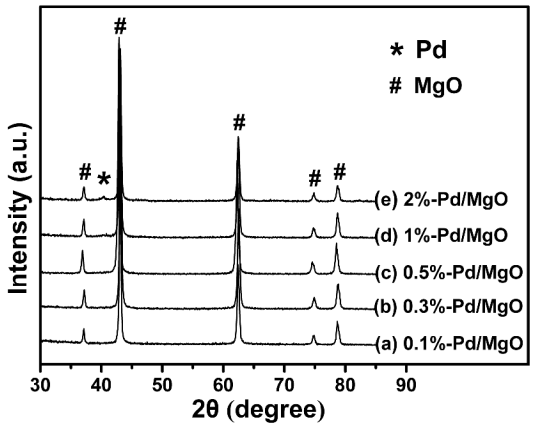

Fig. 4 XRD patterns of Pd/MgO catalysts with different Pd loadings.

UV–DRS investigations are carried out for the characterization of PdO species, Fig. 5a presents the UV–DRS profiles of pure MgO support and the calcined PdO/MgO samples with various PdO loadings. For the pure MgO support, there are no absorption bands observable above 400 nm, while for the PdO/MgO, there is only one broad absorption band with maximum at about 620 nm, which can be assigned to the optical absorption edge of PdO.[23] The Kubelka–Munk function ($\alpha/S = (1-R)^2/2R$) is often used to evaluate the band gap of a semiconductor material in terms of the Tauc plot,[24] which is constructed by plotting the Kubelka–Munk function. The determined band gap of the PdO increases with the increase of PdO loading (Fig. 5b), indicating a blue shift of the absorption edge. There is a significant difference (0.16 eV) on the band gaps between 0.1%-PdO/MgO and 2%-PdO/MgO. The UV-DRS results suggest that the coordination environment of palladium species is changed due to the interaction between PdO and MgO support, which was significantly affected by the PdO loading.

The results of the TPR experiments for the calcined samples (PdO/MgO) are presented in Fig. 6. A single peak was observed for all the calcined samples and the intensity increases gradually along with the increase of the PdO loading. This reveals that the PdO species are reduced to metallic Pd and the amounts of H_2 consumed are closely associated with the PdO loadings. Moreover, it should be noted that the reduction peak position of the maxima shifts towards the higher temperatures from 73–93°C as the PdO loading increases. This shift can be interpreted as the result of the enhancement of the interaction between PdO species and MgO support, deriving from the characterization of UV–DRS. The strong interaction between PdO species and MgO support can effectively prevent the aggregation and sintering of Pd nanoparticles during the the hydrogen reduction process at high temperature, which can be verified by the TEM images (Fig. 3).

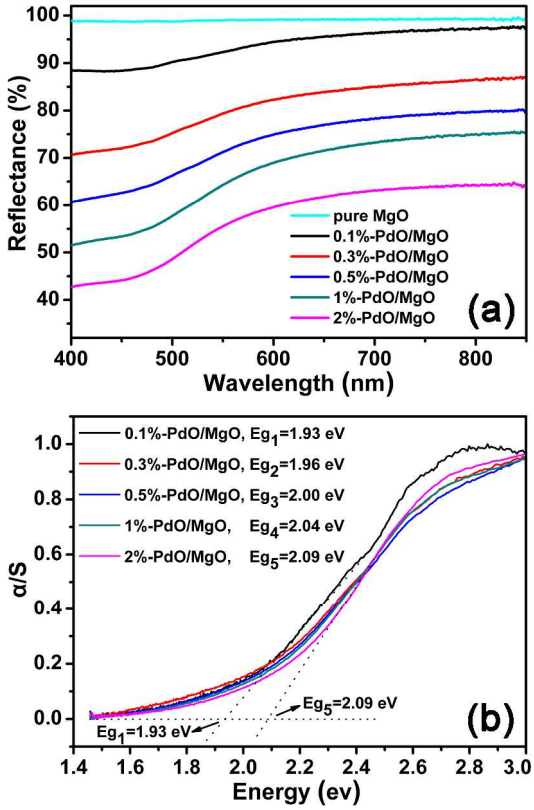

Fig. 5 (a) UV–DRS profiles of pure MgO support and the calcined samples (PdO/MgO); (b) Tauc plots constructed from (a) according to Kubelka–Munk function $\alpha/S = (1-R)^2/2R$: the ordinate values (α/S) have been normalized.

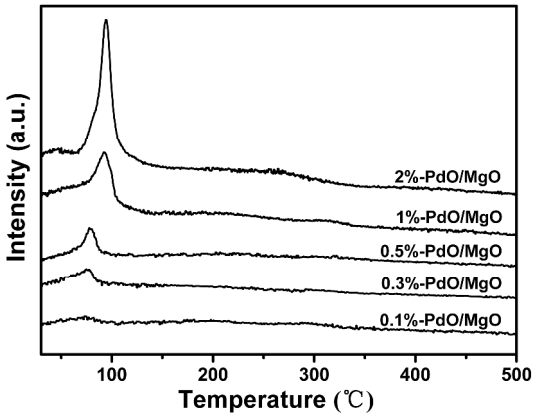

Fig. 6 H_2-TPR profiles of the calcined samples (PdO/MgO).

Fig. 7 displays the TPD profiles of CO_2 adsorbed on pure MgO

support and Pd/MgO catalysts with different Pd loadings. Several CO_2 desorption peaks are observed for all samples, which can be classified into three types of basic sites with different strengths, i.e., ''Weak'' (CO_2 desorption between 27 and 147 °C), ''Medium'' (CO_2 desorption between 147 and 377 °C), and ''Strong'' (CO_2 desorption above 377 °C) basicity.[25] The "weak" basic sites are probably associated with Bronsted basicity and mostly likely arising from the lattice-bound OH groups. The "medium" and "strong" sites are probably correlated to Lewis basicity originating from the three- and four-fold-coordinated O^{2-} anions.[25] The CO_2-TPD profiles of Pd/MgO catalysts are similar to that of the pure MgO support, indicating that the surface basicity sites of MgO support remain unchanged during the preparation of catalysts. A similar phenomenon was also observed by Shen et al.[26]

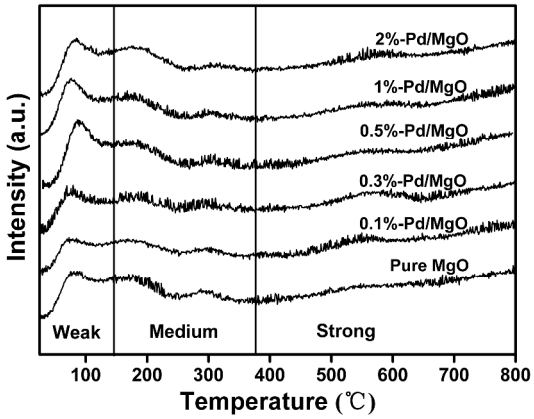

Fig. 7 CO_2-TPD profiles of pure MgO support and Pd/MgO catalysts with different Pd loadings.

4. Conclusions

In summary, we firstly found that the basic MgO can serve as an excellent support used in the Pd catalyst for CO oxidative coupling to DMO. The amount of Pd loading significantly affects the catalytic performance for CO oxidative coupling to DMO. The activity of Pd/MgO catalyst increases with the increase of the Pd loading because of the high dispersion and similar size of Pd nanoparticles, as well as the increase of surface active sites. The low Pd loading catalyst (0.5%-Pd/MgO) exhibits excellent activity, selectivity and stability with 63% CO conversion, 97% selectivity to DMO and more than 120 h on stream at 130 °C. This work provides insight for designing high-performance catalysts for CO oxdiative coupling to DMO by choosing appropriate supports. Further experimental and theoretical studies are still required to gain more insights into the origin of the role of the supports.

Acknowledgements

We gratefully acknowledge financial support from the 973 Program (2011CBA00505, 2013CB933200), and NSF of China (21003126, 21203200, 21303202), and NSF of Fujian Province (2013J05034).

Notes and references

1. T.-J. Zhao, D. Chen, Y.-C. Dai, W.-K. Yuan and A. Holmen, *Ind. Eng. Chem. Res.*, 2004, **43**, 4595-4601.
2. Y.-N. Wang, X. P. Duan, J. W. Zheng, H. Q. Lin, Y. Z. Yuan, H. Ariga, S. Takakusagi and K. Asakura, *Catal. Sci. Technol.*, 2012, **2**, 1637-1639.
3. A.-Y. Yin, X.-Y. Guo, W.-L. Dai and K.-N. Fan, *Chem. Commun.*, 2010, **46**, 4348-4350.
4. Z. He, H. Q. Lin, P. He and Y. Z. Yuan, *J. Catal.*, 2011, **277**, 54-63.
5. J. D. Lin, X. Q. Zhao, Y. H. Cui, H. B. Zhang and D. W. Liao, *Chem. Commun.*, 2012, **48**, 1177-1179.
6. H. R. Yue, Y. J. Zhao, X. B. Ma and J. L. Gong, *Chem. Soc. Rev.*, 2012, **41**, 4218-4244.
7. L. Lin, P. B. Pan, Z. F. Zhou, Z. J. Li, J. X. Yang, M. L. Sun and Y. G. Yao, *Chinese. J. Catal.*, 2011, **32**, 957-969.
8. Z. F. Zhou, Z. J. Li, P. B. Pan, L. Lin, Y. Y. Qin and Y. G. Yao, *Chem. Ind. Eng. Prog.*, 2010, **29**, 2003-2009.
9. D. M. Fenton and P. J. Steinwand, *J. Org. Chem*, 1974, **39**, 701-704.
10. Q. Lin, Y. Ji, Z. D. Jiang and W. D. Xiao, *Ind. Eng. Chem. Res.*, 2007, **46**, 7950-7954.
11. X. G. Zhao, Q. Lin and W. D. Xiao, *Appl. Catal., A*, 2005, **284**, 253-257.
12. Y. Ji, G. Liu, W. Li and W. D. Xiao, *J. Mol. Catal. A: Chem.*, 2009, **314**, 63–70.
13. Z.-N. Xu, J. Sun, C.-S. Lin, X.-M. Jiang, Q.-S. Chen, S.-Y. Peng, M.-S. Wang and G.-C. Guo, *ACS Catal*, 2013, **3**, 118-122.
14. S.-Y. Peng, Z.-N. Xu, Q.-S. Chen, Y.-M. Chen, J. Sun, Z.-Q. Wang, M.-S. Wang and G.-C. Guo, *Chem. Commun.*, 2013, **49**, 5718-5720.
15. S. Uchiumi, K. Ataka and T. Matsuzaki, *J. Organomet. Chem.*, 1999, **576**, 279-289.
16. D. Widmann, Y. Liu, F. Schuth and R. J. Behm, *J. Catal.*, 2010, **276**, 292-305.
17. M. Comotti, W.-C. Li, B. Spliethoff and F. Schuth, *J. Am. Chem. Soc.*, 2006, **128**, 917-924.
18. H. Yoshida, T. Nakajima, Y. Yazawa and T. Hattori, *Appl. Catal.*, B: Environ., 2007, **71**, 70-79.
19. P. Sangeetha, K. Shanthi, K. S. R. Rao, B. Viswanathan and P. Selvam, *Appl. Catal.*, A, 2009, **353**, 160-165.
20. S. Rojluechai, S. Chavadej, J. W. Schwank and V. Meeyoo, *Catal. Commun.*, 2007, **8**, 57-64.
21. T. Nanba, S. M. Asukawa, J. Uchisawa and A. Obuchi, *J. Catal.*, 2008, **259**, 250-259.
22. R. K. Marella, C. K. P. Neeli, S. R. R. Kamaraju and D. R. Burri, *Catal. Sci. Technol.*, 2012, **2**, 1833-1838.
23. C.-J. Huang, F.-M. Pan, H.-Y. Chen and L. Chang, *J. Appl. Phys.*, 2010, **108**, 053105.
24. J. Tauc, R. Grigorovici and A. Vancu, *Phys. Status Solidi*, 1966, **15**, 627-637.
25. Z. Liu, J. A. Cortes-Concepcion, M. Mustian and M. D. Amiridis, *Appl. Catal., A*, 2006, **302**, 232-236.
26. S. Li, C. H. Chen, E. S. Zhan, S.-B. Liu and W. J. Shen, *J. Mol. Catal. A: Chem.*, 2009, **304**, 88-94.